Available online at www.sciencedirect.com
ScienceDirect
Journal of Molecular Spectroscopy 243 (2007) 1–9
Journal of MOLECULAR SPECTROSCOPY
www.elsevier.com/locate/jms

The rotational spectrum of chlorine nitrate ($ClONO_2$): The v_5/v_6v_9 dyad

Rebecca A.H. Butler [a], Douglas T. Petkie [b], Paul Helminger [c], Frank C. De Lucia [d,*], Zbigniew Kisiel [e]

[a] Department of Physics, Pittsburg State University, Pittsburg, KS 66726, USA
[b] Department of Physics, Wright State University, Dayton, OH 45435, USA
[c] Department of Physics, University of South Alabama, Mobile, AL 36688, USA
[d] Department of Physics, The Ohio State University, Columbus, OH 43210-1106, USA
[e] Institute of Physics, Polish Academy of Sciences, Al. Lotników 32/46, 02-668 Warszawa, Poland

Received 5 January 2007; in revised form 21 February 2007
Available online 3 March 2007

Abstract

Chlorine nitrate is a molecule of both spectroscopic and atmospheric interest. It is a species whose spectrum in the infrared is marginally resolved in the Doppler limit, thereby limiting the spectroscopic study of its dense rovibrational structure. Analyses of its pure rotational spectrum in the millimeter and submillimeter (mm/submm) spectral regions of the ground, v_9, $2v_9$, v_7, $3v_9$, and v_7v_9 vibrational states have been previously reported. In this paper, we report the recording of a new 'complete' mm/submm spectrum from 78 to 378 GHz using phase-lock and FASSST (FAst Scan Submillimeter Spectroscopic Technique) systems. We also report the use of these new data for redetermination of spectroscopic constants for the ground state and for an analysis of the v_5/v_6v_9 interacting dyad, whose corresponding infrared spectrum lies near 560 cm^{-1}. The simulation of the rotational structure of v_5 from the mm/submm analysis is of particular interest because it is one of the bands that is used for atmospheric remote sensing.

Keywords: Chlorine nitrate; $ClONO_2$; Millimeter; Spectra; Spectroscopy; Remote sensing; Atmosphere

1. Introduction

Chlorine nitrate ($ClONO_2$) is a planar, near prolate molecule ($\kappa \sim -0.9$) with a strong *a*-axis dipole moment, $\mu_a = 0.72(7)$D, and a weaker *b*-axis component, $\mu_b = 0.24(2)$ [1]. Its importance in atmospheric chemistry has been widely noted [2–6]. In natural abundance the two chlorine isotopologues, $^{35}ClONO_2$ and $^{37}ClONO_2$, are of greatest importance, each with several low-lying vibrational states. This creates a very complex and crowded pure rotational spectrum in the millimeter and submillimeter (mm/submm) spectral region and a marginally resolved infrared spectrum.

The character of the vibrational fundamentals has been established by Miller et al. [7] and a harmonic force field calculated from measured vibrational fundamentals [5]. High-resolution infrared work has been done on v_4, v_5, and v_2 [4,6,8,9]. Several microwave studies have been done of the ground and v_9 states [1,10,11]. More recently, microwave work has also been reported on the lowest energy dyads of interacting vibrational states, including $2v_9/v_7$ [12] and $3v_9/v_7v_9$ [12,13], and relations among the spectral constants and Fermi resonances of the several vibrational interactions were developed [14].

Because the rotational structure of chlorine nitrate's infrared bands has been difficult to establish, remote sensing recoveries are currently based on band spectra approaches rather than line-by-line calculations [15]. A typical technique has been to approximate the observed cross section by the use of a set of equally spaced spectral lines of varying intensity whose lower energy levels are selected to provide an appropriate temperature dependence [6,16]. Reports of line-by-line analyses of infrared spectra

* Corresponding author.
E-mail address: fcd@mps.ohio-state.edu (F.C. De Lucia).

0022-2852/$ - see front matter © 2007 Published by Elsevier Inc.
doi:10.1016/j.jms.2007.02.023

are beginning to appear. The most successful of these have been based on cooled molecular beams with reduced spectral density [4,9], but the low temperature of these beams does not allow modeling of the spectrum at atmospheric temperatures. Additionally, analyses of resolved lines and band contours have been used to provide the bases for simulations and atmospheric retrievals [17].

One of the motivations for the work reported here is to use the higher resolution in the mm/submm region to resolve this otherwise difficult to observe rotational structure and to develop quantum mechanical spectroscopic models. We have shown in the case of the spectrally complex $\nu_5/2\nu_9$ dyad of HNO_3 [18] that the knowledge of the rotational structure of the relevant excited states that can be obtained from the mm/submm spectrum is sufficient to calculate its rotational energy level structure to very high accuracy. We have also used this approach to simulate the rotational structure of the infrared bands of HNO_3 in the 22 μ region [19].

However, this mm/submm approach faces its own difficult, if somewhat less fundamental, challenges. First, the pure rotational spectra in excited vibrational states are effectively hot bands and their intensities are reduced by their corresponding Boltzmann factor. However, the sensitivity of modern mm/submm spectroscopy is such that even high lying levels are of sufficient intensity to be observed. For example, we have measured and analyzed the ν_2 state of HNO_3 near 1700 cm^{-1} with integration times of $\sim 10^{-3}$ s.

The greater challenge is spectral confusion because the rotational spectra in all vibrational states for all isotopic species occupy the same spectral space. For this reason we started our analyses of $ClONO_2$ with the lowest lying vibrational states and extended the earlier analyses to higher lying rotational states. This left the lines for each successive analysis among the strongest unassigned lines. While ν_6 and the $4\nu_9/\nu_7 2\nu_9/2\nu_7$ triad are lower in energy than the $\nu_5/\nu_6\nu_9$ interacting pair reported here, we have preliminary analyses of the lower states that allowed this work to proceed without great difficulty.

The present work focuses on the $\nu_5/\nu_6\nu_9$ interacting pair because ν_5 is particularly well suited for atmospheric observations and because $\nu_6\nu_9$ is the upper state of the first hot band of ν_6—another state of importance for atmospheric remote sensing. Thus, the interacting pair discussed in this paper is important for the development of line-by-line models that are capable of simulating the infrared spectra of both of these bands at arbitrary atmospheric temperature.

2. Experiment

2.1. The FASSST spectrometer

The work which we have previously reported on $ClONO_2$ was based on single FASSST (FAst Scan Submillimeter Spectrometer Technique) [20] scans (with analog integration times of $\sim 10^{-5}$ s), along with slow scans (with an analog integration time of ~1 s) taken with a phase locked instrument between 78 and 118 GHz [14,21,22]. The initial assignments and analyses reported in this paper are also based on these data. However, to broaden the experimental base for this work to more of the rotational manifold (and to make possible analyses of yet higher vibrational states), we recorded new FASSST spectra between 118 and 378 GHz. These new data are based on 400 co-added scans (an effective integration time of $\sim 10^{-3}$ s). This was combined with an improved sample preparation, increasing the S/N of the spectrum by ~100. There is only a small, 8 GHz segment of the rotational spectrum at 185.58–193.48 GHz, which for technical reasons is missing in the FASSST spectrum.

2.2. Chemical synthesis

The chlorine nitrate was synthesized using the reaction between chlorine monofluoride and lead nitrate [23].

$$2ClF + Pb(NO_3)_2 \rightarrow PbF_2 + 2ClONO_2$$

The presence of water in the lead nitrate resulted in the production of nitric acid. However, its higher vapor pressure allowed most of it to be distilled from the sample and the remainder was used as a calibration gas for the spectrometer.

3. The spectroscopy of the $\nu_5/\nu_6\nu_9$ dyad

3.1. Infrared laboratory work

The ν_5 band in the infrared has been studied in the laboratory at near stratospheric conditions (233 K). These results were then compared with actual stratospheric observations [6], which came from regions of the stratosphere which ranged in temperature from 207 to 253 K at the time of the observations.

3.2. Spectral simulation strategy

As noted above, the infrared spectrum of chlorine nitrate is difficult to characterize for atmospheric retrievals because it represents an awkward resolution case. It is not well enough resolved for laboratory analysis to provide a detailed spectral analysis, but nonetheless has a complicated, partially resolved signature that is not well characterized by a simple knowledge of the integrated band strength. For the aforementioned comparison, the cross section was approximated by creation of a set of synthetic equi-spaced spectral lines, whose ground state energies were adjusted to reproduce the observed temperature dependence of the integrated cross section. This temperature dependence was obtained from Davidson et al. [24].

3.3. Simulation from pure rotational data

The work reported here provides an alternative approach. In spite of the substantial mixing with v_6v_9 that complicates the spectrum of v_5 at high resolution, the mm/submm pure rotational spectrum reported here makes possible a detailed analysis of both vibrational states of the dyad. This analysis, combined with the reanalyzed ground state, makes possible the simulation of the v_5 band to very high accuracy at arbitrary atmospheric temperature.

Because the spectroscopy of a particular set of mixed states involves analyses that (because of hot band contributions) ultimately will be involved in the simulations of *different* infrared regions, the availability of data for these simulations does not neatly track the completion of spectroscopic analyses. For example, the infrared region around v_5 also contains hot bands such as $(v_5 + v_9 - v_9)$ which we have yet to analyze, but the region around v_6 (for which we have a reasonably good analysis based on the original data set) contains the hot bands $(v_6 + v_9 - v_9)$. This hot band can be synthesized based on the analysis of the v_6v_9 part of the dyad reported here.

While the hot band problem is in some sense infinite, in preliminary work we have found that reasonably good results can be obtained if only the fundamental band is analyzed in detail and low-resolution band contours are generated for the hot bands based on the expected progressions of spectroscopic parameters as a function of the vibrational state quantum numbers. If, as in the case of the region around v_6, the detailed spectroscopy of both the fundamental and of the first hot band is known, we expect that the results will be very satisfactory.

4. Results and analysis

In this work, we report the analyses of the pure rotational spectra of the $v_5 = 1$ and $(v_6 = 1,\ v_9 = 1)$ states. $v_5 = 1$ gives rise to infrared spectrum in the 540–580 cm^{-1} region. While the room-temperature rotational spectra of these states are weaker in the mm/submm region by about a factor of 15 in comparison to those of the ground vibrational state, they are still strong and well resolved. The principal challenge to their analysis is the strong perturbation between the two states, which was found to affect rotational transitions with low values of the K_a quantum number. The interactions between the states of the v_5/v_6v_9 dyad are different than those which we have reported previously for the $v_7/2v_9$ [12] and the $v_7v_9/3v_9$ [13] dyads because the current states are of different symmetry and in the v_5/v_6v_9 dyad there is, therefore, no first order Fermi interaction to push the states apart. The $v_5 = 1$ state belongs to the A' and the $(v_6 = 1,\ v_9 = 1)$ state to the A'' representation of the C_s symmetry group for the $ClONO_2$ molecule, so that Coriolis coupling between the two states is possible about both the *a*- and the *b*-inertial axes. The interaction is expected to be prominent due to relatively small vibrational energy difference between the states, which was estimated from the fitted harmonic force field to be close to 8 cm^{-1} for $^{35}ClONO_2$ [11].

The Hamiltonian for the analysis was constructed in standard block-wise manner, in which we have used Watson's asymmetric rotor Hamiltonian [25] for the diagonal terms for the two vibrational states, and an interstate off-diagonal coupling term of the form

$$H_{\mathrm{cor}} = (G_a + G_a^J P^2 + G_a^K P_z^2 + \ldots)P_z + (G_b + G_b^J P^2 + \ldots)P_x. \quad (1)$$

The truncation of the centrifugal distortion expansions for G_a and G_b in Eq. (1) is made at the number of terms that proved to be sufficient for describing the observed perturbation to experimental accuracy. The next higher order terms involving coefficients $F_{\beta\gamma}$ of angular momentum operators $P_\beta P_\gamma + P_\gamma P_\beta$ did not prove necessary. In dealing with Coriolis perturbations several different choices of constants of fit can lead to similar deviations of fit, and the choice used presently has been selected since it is based on the constants associated with lowest order angular momentum operators uses the smallest number of constant of fit, and is characterized by relatively small intercorrelations between the constants. The fits and predictions were performed with Pickett's SPFIT/SPCAT package [26,27]. In addition to the presence of strong Coriolis interaction, there are further complications in the analysis. In natural abundance the spectra of both ^{35}Cl and ^{37}Cl isotopologues are of importance. Furthermore, in the room-temperature spectrum there are ten vibrational states for each isotopologue that are lower in energy than the states in the studied dyad, so that rotational transitions in the lower states have to be accounted for. For this reason the assignment and construction of the datasets were carried out with the help of the AABS package for Assignment and Analysis of Broadband Spectra [28,29]. The package provides mechanisms for keeping track of previously assigned states, is optimized for efficient processing of very extended spectra, and provides Loomis–Wood type tools for graphical assignment.

4.1. The ground vibrational state

Since the vibrational states of interest are at ~550 cm^{-1}, it is natural that fewer transitions can be observed than in the ground vibrational state. In consequence, some of the higher order constants in the Hamiltonian are not determinable and have to be fixed at values for the ground state, so that reliable ground state constants are required for this purpose. We have used our new spectra to improve our previously published ground state analysis. The datasets were considerably extended by combining transitions measured in the new spectra with those used in Ref. [11]. The resulting spectroscopic constants are reported Table 1 for the *S*-reduced form of Watson's Hamiltonian, and in Table 2 for the *A*-reduced Hamiltonian, which has not previously been used. The complete data files for $^{35}ClONO_2$ are

Table 1
Comparison of the *S*-reduced spectroscopic constants determined for the ground state and for the ($v_6 = 1$, $v_9 = 1$) and $v_5 = 1$ states in $^{35}ClONO_2$ and $^{37}ClONO_2$

		$^{35}ClONO_2$			$^{37}ClONO_2$		
		g.s.	($v_6 = 1$, $v_9 = 1$)	$v_5 = 1$	g.s.	($v_6 = 1$, $v_9 = 1$)	$v_5 = 1$
A	/MHz	12105.78277(23)[a]	12016.5184(87)	12052.1542(78)	12105.32502(32)	12016.921(12)	12050.764(13)
B	/MHz	2777.000768(39)	2767.09804(17)	2769.26604(18)	2700.973934(37)	2691.66427(26)	2693.35023(26)
C	/MHz	2258.151163(37)	2254.14031(17)	2248.40813(19)	2207.604555(35)	2203.89052(21)	2197.98329(25)
D_J	/kHz	0.500743(10)	0.516907(34)	0.506687(35)	0.4810004(97)	0.495978(43)	0.486942(47)
D_{JK}	/kHz	3.854253(83)	3.89647(82)	3.81895(81)	3.71562(11)	3.7438(31)	3.6919(31)
D_K	/kHz	9.4738(16)	8.305(49)	9.452(47)	9.6419(34)	8.79(11)	9.30(13)
d_1	/kHz	−0.0957017(60)	−0.096530(10)	−0.098634(10)	−0.0896618(57)	−0.090298(18)	−0.092432(24)
d_2	/kHz	−0.0177421(29)	−0.0170412(61)	−0.0180775(67)	−0.0161924(30)	−0.015497(12)	−0.016560(14)
H_J	/Hz	−0.0001361(10)	−0.0001570(33)	−0.0001432(33	−0.00012483(92)	−0.0001346(40)	−0.0001252(42)
H_{JK}	/Hz	−0.005812(11)	−0.005248(80)	−0.005268(79)	−0.005504(12)	[−0.005504]	[−0.005504]
H_{KJ}	/Hz	−0.015042(56)	[−0.01504]	[−0.01504]	−0.01488(10)	[−0.01488]	[−0.01488]
H_K	/Hz	0.0391(25)	[0.03915]	[0.03914]	0.0367(58)	[0.0367]	[0.0367]
h_1	/Hz	−0.00002388(73)	[−0.00002388]	[−0.00002388]	−0.00002142(63)	[−0.00002142]	[−0.00002142]
h_2	/Hz	−0.00000446(43)	[−0.000004463]	[−0.000004463]	−0.00000297(43)	[−0.00000297]	[−0.00000297]
h_3	/Hz	0.00000472(25)	[0.000004716]	[0.000004716]	0.00000457(23)	[0.00000457]	[0.00000457]
$3\chi_{aa}/2$	/MHz	−125.907(60)			−99.121(93)		
$(\chi_{bb}-\chi_{cc})/4$	/MHz	−11.130(13)			−8.699(14)		
χ_{ab}	/MHz	74.216(47)			58.539(80)		
ΔE	/MHz		123653.97(18)			160209.85(29)	
	/cm^{-1}		4.124652(6)			5.344025(10)	
G_a	/MHz		1644.529(43)			1680.256(75)	
G_a^J	/kHz		−2.323(27)			−2.232(29)	
G_a^K	/kHz		21.3(10)			12.7(14)	
G_b	/MHz		401.5822(54)			396.646(10)	
G_b^J	/kHz		0.0445(15)			0.0815(30)	
N_{lines}		2810	2274		2119	979	
σ_w[b]		0.5677	0.6877		0.5243	0.6676	
σ_{fit}	/kHz	44.9	68.8		40.7	66.8	

[a] The quantities in round parentheses are standard errors in units of the least significant digit of the value of the constant. Square parentheses denote assumed values, taken from the ground state for the same isotopologue.

[b] Weighted deviation of the fit, in which synthesizer lines were assigned measurement error of 50 kHz, and FASSST lines an error of 100 kHz and a cutoff criterion of four times experimental error was applied for inclusion of lines in the fit.

included in Table S1 of the supplementary electronic information, and for $^{37}ClONO_2$ in Table S2. Although the reanalysis was targeted at deriving a full set of reliable sextic order spectroscopic constants, the fits included both hyperfine resolved and hyperfine unresolved transitions, and lead to improvement also of the nuclear quadrupole coupling constants for the chlorine nucleus in both isotopologues.

4.2. The v_5/v_6v_9 dyad

After initial assignments, Loomis–Wood type graphical displays were used to identify the low K_a line sequences in the FASSST spectrum. These results were augmented by initially using the ground state centrifugal distortion parameters and simulations as aids for the identification of additional lines. The interstate coupling required only the several leading terms in the centrifugal series based on G_a and G_b, as listed in Eq. (1). A total of 2274 lines in the ^{35}Cl isotopologue and 979 lines in the ^{37}Cl isotopologue were assigned and analyzed. The resulting spectroscopic constants are reported in Tables 1 and 2, and the associated data files are in Tables S3–S6 of the supplementary electronic information. In the end, the final solution turned out to be deceptively simple: the quartic constants for the two excited states are very close to those of the ground state, and only five interaction constants plus the vibrational energy difference ΔE allow a fit of everything we can unambiguously identify in the spectrum.

For the ground state, the *S*-reduced fit is somewhat better than the *A*-reduced fit, while for the excited states, it is the fit with the *A*-reduced Hamiltonian that is marginally better for the ^{35}Cl isotopologue. There is no distinction for the ^{37}Cl isotopologue. The *A*-reduced form of the fit was the method of choice while searching the highly nonlinear solution space for the global minimum since it was found to be more stable numerically and was faster in execution time. All rotational transitions assigned in each of the two excited vibrational states are of the ^aR-type, and for the ^{35}Cl isotopologue the assigned lines go up to $K_a = 22$, while for ^{37}Cl it was decided not to proceed beyond $K_a = 10$. This results from a conservative approach

Table 2
Comparison of the A-reduced spectroscopic constants determined for the ground state and for the ($v_6 = 1$, $v_9 = 1$) and $v_5 = 1$ states in $^{35}ClONO_2$ and $^{37}ClONO_2$

		$^{35}ClONO_2$			$^{37}ClONO_2$		
		g.s.	($v_6 = 1$, $v_9 = 1$)	$v_5 = 1$	g.s.	($v_6 = 1$, $v_9 = 1$)	$v_5 = 1$
A	/MHz	12105.78248(24)	12016.5333(86)	12052.1520(77)	12105.32469(32)	12016.935(12)	12050.760(13)
B	/MHz	2777.006065(39)	2767.10311(17)	2769.27165(18)	2700.979047(37)	2691.66921(26)	2693.35571(26)
C	/MHz	2258.145973(38)	2254.13538(17)	2248.40269(18)	2207.599536(35)	2203.88562(21)	2197.97810(25)
Δ_J	/kHz	0.536220(11)	0.551036(34)	0.542802(36)	0.513380(10)	0.527021(44)	0.520027(54)
Δ_{JK}	/kHz	3.641190(97)	3.69165(79)	3.60223(78)	3.52110(12)	3.5599(29)	3.4923(30)
Δ_K	/kHz	9.6515(16)	8.553(49)	9.697(47)	9.8040(35)	8.93(11)	9.56(13)
δ_J	/kHz	0.0957016(61)	0.0965415(99)	0.0986273(98)	0.0896601(57)	0.090329(17)	0.092416(24)
δ_K	/kHz	2.62288(45)	2.52778(90)	2.65076(97)	2.53422(49)	2.4351(20)	2.5692(22)
ϕ_J	/Hz	−0.0001451(12)	−0.0001639(33)	−0.0001534(33)	−0.0001309(10)	−0.0001422(40)	−0.0001310(42)
ϕ_{JK}	/Hz	−0.00323(14)	−0.002720(79)	−0.002582(78)	−0.00271(14)	[−0.00271]	[−0.00271]
ϕ_{KJ}	/Hz	−0.02372(49)	[−0.02372]	[−0.02372]	−0.02438(49)	[−0.02438]	[−0.02438]
ϕ_K	/Hz	0.0455(26)	[0.0455]	[0.0455]	0.0436(58)	[0.0436]	[0.0436]
ϕ_J	/Hz	−0.00001911(72)	[−0.00001911]	[−0.00001911]	−0.00001688(63)	[−0.00001688]	[−0.00001688]
ϕ_{JK}	/Hz	−0.001640(64)	[−0.00164]	[−0.00164]	−0.001419(68)	[−0.001419]	[−0.001419]
ϕ_K	/Hz	0.0421(36)	[0.0421]	[0.0421]	0.0521(38)	[0.0521]	[0.0521]
$3\chi_{aa}/2$	/MHz	−125.907(61)			−99.119(93)		
$(\chi_{bb}-\chi_{cc})/4$	/MHz	−11.131(13)			−8.700(14)		
χ_{ab}	/MHz	74.216(48)			58.544(80)		
ΔE	/MHz		123654.28(18)			160209.98(29)	
	/cm^{-1}		4.124663(6)			5.344030(10)	
G_a	/MHz		1644.697(43)			1680.515(75)	
G_a^J	/kHz		−2.355(27)			−2.360(29)	
G_a^K	/kHz		24.3(10)			19.9(14)	
G_b	/MHz		401.5692(53)			396.637(10)	
G_b^J	/kHz		0.0250(15)			0.0538(29)	
N_{lines}		2810	2274		2119	979	
σ_w		0.5710	0.6809		0.5287	0.6681	
σ_{fit}	/kHz	45.2	68.1		40.8	66.8	

to assignment in which only clearly visible sequences of adjacent lines with the correct intensity/lineshape are regarded as trustworthy. The intensity of the two excited states for the ^{37}Cl species corresponds to vibrational energy of about 800 cm^{-1} for the parent. We expect, therefore, that as we complete our analyses of the new data sets for higher lying triads such as $4\nu_9/\nu_7 2\nu_9/2\nu_7$ near 500 cm^{-1} and $5\nu_9/\nu_7 3\nu_9/2\nu_7\nu_9$ near 620 cm^{-1} (for which we have preliminary analyses based on the original single scan data set), that we will be able to reliably assign significantly weaker lines because there will be fewer unassigned lines left in the assignment pool.

The scope of the data set acquired for the $^{35}ClONO_2$ isotopologue and the accuracy to which the measured frequencies are reproduced by the fitted constants are illustrated in the bottom two distribution plots in Fig. 1. With a few exceptions, the deviations from the fits are random, as one might expect for a fit with an overall weighted deviation of below unity. There is only one sequence of lines, $K_a'' = 18$ for $\nu_6\nu_9$ (the lower of the two interacting vibrational states), that diverges systematically at the highest J. All other instances of large obs.−calc. differences are scattered. It is most likely that the deviations apparent for $\nu_6\nu_9$ are due to anharmonic resonances with other states, and one possible candidate is $2\nu_7$. This is the topmost state in the $4\nu_9/\nu_7 2\nu_9/2\nu_7$ triad and is closest in energy to the studied dyad, lying *ca* 30 cm^{-1} below $\nu_6\nu_9$. The lack of a similar perturbation at high K_a in the ^{37}Cl isotopologue may possibly be the reason for some differences between fitted values for the perturbation constants in the two isotopologues as in the parent the fit may possibly be trying to encompass in an effective way behavior that is outside the assumed model.

4.3. Overview of the perturbation

It has already been mentioned that the perturbation affects rotational transitions with relatively low values of K_a. A very useful overview of the nature of the perturbations in the investigated dyad is provided by plots based on values of mixing coefficients, as in the upper two panes in Fig. 1. The value of the mixing coefficient, P_{mix}, for a given energy level will range from unity in the absence of perturbation to 0.5 for the case of complete two state mixing. The quantity $1-P_{mix}$ plotted in Fig. 1 is therefore a useful measure of the magnitude of the perturbation affecting a given level. The plots are made from the output of the SPCAT program, generated on the basis of the final fit. It is

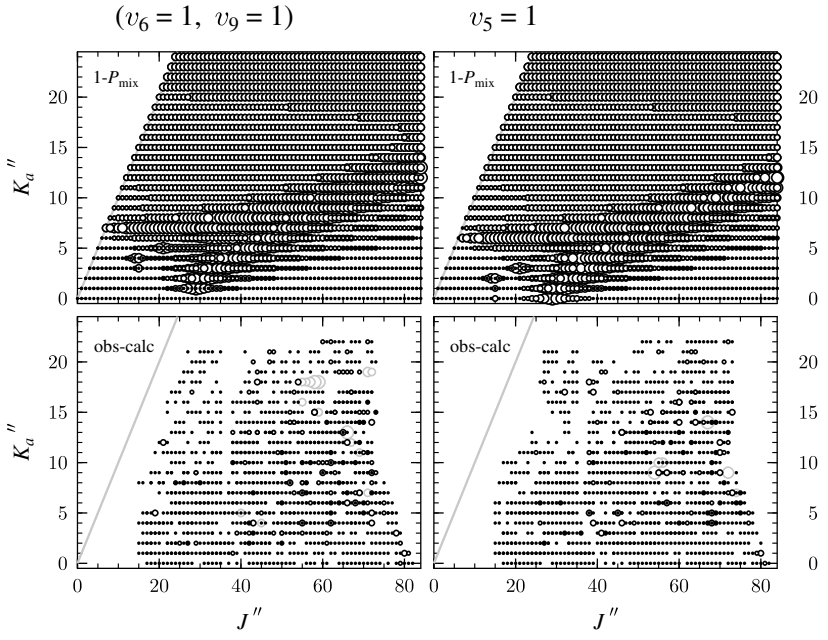

Fig. 1. Dataset distribution plots as a function of quantum numbers J'' and K_a'' for rotational transitions in the $(v_6 = 1,\ v_9 = 1)$ and $v_5 = 1$ interacting vibrational states in $^{35}ClONO_2$. The two lower panes depict values of obs.−calc. differences and the two upper panes depict the degree of mixing between a given rotational level in one vibrational state with a rotational level in the second state, as defined by the quantity $1-P_{mix}$ (see text). Circle diameters in the lower plot are proportional to the magnitudes of the values of obs.−calc. and are chosen such that the black circles are all for obs.−calc. <0.3 MHz. In the upper panes circle diameters range from the smallest for $1-P_{mix} < 0.005$ to the largest for $1-P_{mix} > 0.1$.

apparent that lines with lowest values of J and K_a will be relatively unaffected by the perturbation, and this was in fact the reason why initial assignment of these states was relatively straightforward. Nevertheless, very extended islands of perturbation are encountered at relatively small values of the pertinent quantum numbers, with one fork extending down to $K_a = 0$ at $J'' = 29$. Comparison of the upper and lower plots in Fig. 1 shows that the perturbation regions are well represented by lines in the dataset and that the perturbation effects are fitted satisfactorily, since there is no discernible correlation between the trends in the obs.−calc. values and orientation of the two main islands of perturbation.

Further insight into the nature of the perturbation is given by the two difference frequency plots shown in Fig. 2, which correspond to horizontal sections through the plots in Fig. 1. The mirror nature of the two curves in Fig. 2, both as a function of amplitude and of the position of their main features as a function of J, is evidence that they are for coupled sequences of lines in the two states, which differ by 1 in K_a. The central peaks correspond to perturbations of more than 9 GHz and thus there is very little chance of identifying the corresponding line, whereas lines on the sidelobes to both sides of the central peak can be assigned, even though these also result from appreciable perturbations reaching 1 GHz in magnitude. Confident assignment is, however, possible on the basis of the perturbation induced quadrupole structure, as previously seen for the $2v_9/v_7$ dyad [12]. The near-complete nature of the FASSST spectrum allows the dependence of perturbation induced quadrupole structure to be followed

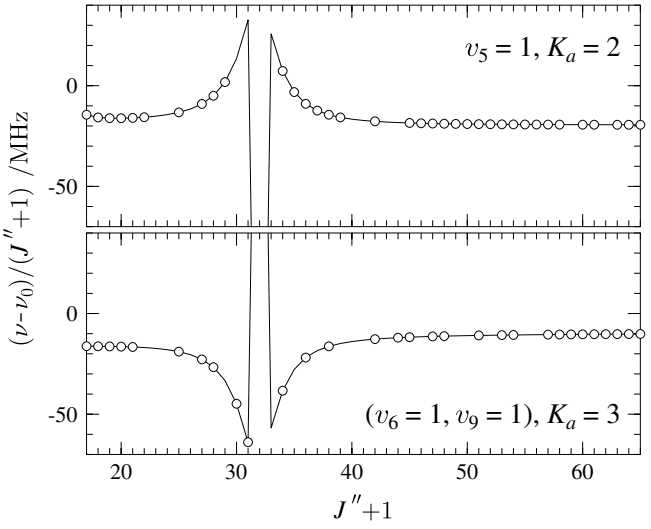

Fig. 2. Illustration of the mirror-image dependence of the Coriolis interaction between $K_a = 3$ ^aR-type transitions in $(v_6 = 1,\ v_9 = 1)$ and $K_a = 2$ transitions in $v_5 = 1$ in $^{35}ClONO_2$. The plots are of a frequency difference between an excited state transition and a corresponding transition in the ground state. The continuous line is based on calculated frequencies, and the circles denote measured lines. For each pair of coupled rotational transitions both upper and lower levels interact and the maximum of the perturbation occurs for the $32_{3,30} \leftarrow 31_{3,29}$ transition in $(v_6 = 1,\ v_9 = 1)$ and the $32_{2,31} \leftarrow 31_{2,30}$ transition in $v_5 = 1$, for which all four levels are calculated to have mixing coefficients close to 0.6.

in some detail, as illustrated in Fig. 3. The splitting of 1–2 MHz appearing in the vicinity of the perturbation maximum is comparable in magnitude to that for the lowest dyad [12]. It is more pronounced than a similar effect

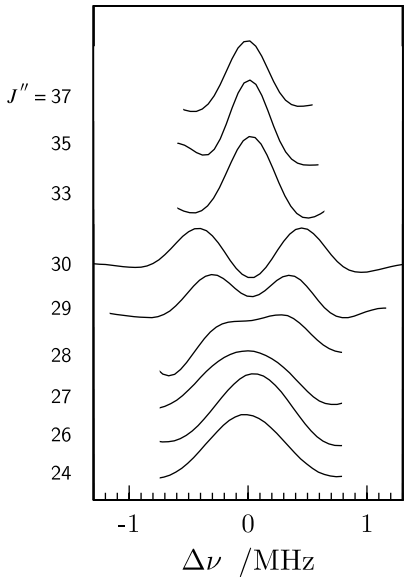

Fig. 3. Evolution of the observed nuclear quadrupole splitting in $K_a = 3$ ^aR-type transitions in the ($v_6 = 1$, $v_9 = 1$) excited vibrational state of $^{35}ClONO_2$ induced by perturbation of this state with the $v_5 = 1$ state. The perturbation maximum is for the $32_{3,30} \leftarrow 31_{3,29}$ transition, but the magnitude of the perturbation is in this case so large (over 9 GHz) that confident assignment is not possible. The next higher transition, for $J'' = 32$, is obscured by a much stronger line.

observed for $CHClF_2$ [30], although much more spectacular manifestations of this type have also been observed, for example for NOBr [31].

In the final stage of the analysis, it became possible to also assign interstate transitions connecting rotational levels in the two vibrational states in the dyad. Such transitions become allowed by the perturbation and their intensity is greatest when the participating energy levels are close to the perturbation maxima. Furthermore, the strongest interstate transitions show much increased nuclear quadrupole structure, in similarity to the most perturbed transitions in Fig. 3. The characteristic splitting patterns provide confirmation of the assignment, and two such transitions for $^{35}ClONO_2$ are visible in the small segment of the FASSST spectrum displayed in Fig. 4. A list of interstate transitions assigned for $^{35}ClONO_2$ is given in Table 3 and is comprised of transitions both from and to each of the states in the dyad.

4.4. Confirmation of vibrational assignment

In the cases for which there is no rotational analysis of the structure of the infrared bands, the identification of an assigned pure rotational state with a particular infrared band must rely on other methods. Intensities of newly assigned rotational transitions relative to those for similar transitions in the several already identified vibrational states are a useful first indicator. Additionally, as one starts with the several polyad combinations involving the two lowest frequency modes, v_9 and v_7, the rotational progressions (expressed either in terms of spectral constants or locations in frequency of similar lines) are relatively well defined [12]. Moreover, the states of each polyad are linked together via the perturbation analyses, thereby reducing the number of variables [14]. Finally, for a planar molecule, the inertial defect is readily calculable from the harmonic force field, and is an extremely useful quantity in assignment.

Table 4 summarizes the principal evidence that we now have for assigning the states studied in this work. The inertial defects for the two states derived from the rotational constants in Tables 1,2 are in excellent agreement with calculation. The magnitude and the sign of the small isotopic change in the inertial defect are also in good agreement between experiment and calculation, as evident from the two rightmost columns in Table 4. The relative ordering in energy of the two states turns out to be as predicted, and although the experiment and calculation differ by a factor of two in the value for the energy difference ΔE, the magnitude of this difference is only several cm^{-1}, so that the agreement is very good. The values in Table 4 demonstrate that the isotopic change in ΔE is also well understood.

5. Summary

This paper reports the analysis to microwave accuracy of about 3000 transitions of the mm/submm pure rota-

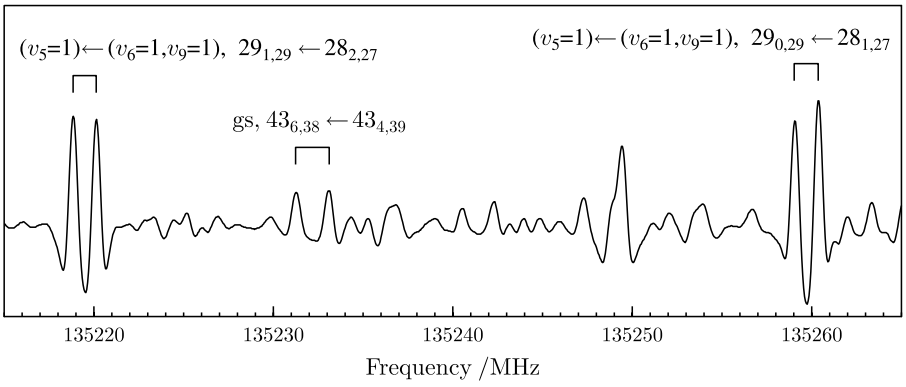

Fig. 4. Two examples of observed interstate transitions between the ($v_6 = 1$, $v_9 = 1$) and $v_5 = 1$ interacting vibrational states in $^{35}ClONO_2$. Unambiguous assignment is possible on the basis of perturbation induced nuclear quadrupole hyperfine splitting, which approaches in magnitude the splitting for the nearby Q-type transition for the $^{35}ClONO_2$ ground state.

Table 3
The assignments, frequencies and residuals (MHz) of selected transitions between vibrational states in the v_5/v_6v_9 dyad in $^{35}ClONO_2$

$v_5 = 1 \leftarrow (v_6 = 1, v_9 = 1)$								$(v_6 = 1, v_9 = 1) \leftarrow v_5 = 1$							
J'	K'_a	K'_c	J''	K''_a	K''_c	obs.	obs.−calc	J'	K'_a	K'_c	J''	K''_a	K''_c	obs.	obs.−calc.
29	1	29	28	2	27	135219.494	0.070	29	2	28	28	1	28	134853.018	0.026
29	0	29	28	1	27	135259.720	0.064	29	1	28	28	0	28	134844.241	0.121
32	2	31	31	3	29	152979.442	0.011	32	2	30	31	1	30	153125.197	0.031
35	2	33	34	4	31	170998.943	−0.005	35	4	32	34	3	32	171180.805	−0.063
34	4	30	33	6	28	175261.192	0.000	34	6	29	33	4	29	174381.607	0.002
41	4	37	40	6	35	206554.183	−0.019	36	3	33	35	3	33	176442.270	0.144
42	6	37	41	7	35	214649.331	−0.070	40	4	36	39	4	36	199496.591	0.029
49	5	44	48	6	42	250176.851	−0.023	39	8	31	38	7	31	200531.414	−0.059
54	6	48	53	7	46	278473.541	−0.030	42	7	36	41	6	36	214287.328	0.006
59	9	50	58	10	48	309120.646	0.094	44	5	39	43	5	39	222239.061	−0.029
60	7	53	59	8	51	310109.541	0.040	54	7	47	53	7	47	277147.593	−0.011
66	8	58	65	9	56	341974.986	−0.178	66	9	57	65	9	57	341950.570	−0.003
67	10	57	66	11	55	351480.298	0.025								

Table 4
Comparison of values for the inertial defect and energy separation for the two states in the v_5/v_6v_9 dyad

		$^{35}ClONO_2$		$^{37}ClONO_2$		^{35}Cl–^{37}Cl	
		obs.	calc.[a]	obs.	calc.	obs.	calc.
Δ_i $(v_6 = 1, v_9 = 1)$[b]	/uÅ^2	−0.49444(4)	−0.4963	−0.49959(5)	−0.5006	0.00515(6)	0.0043
Δ_i $(v_5 = 1)$	/uÅ^2	0.34452(4)	0.3302	0.35237(6)	0.3385	−0.00785(7)	−0.0083
ΔE[c]	/cm^{-1}	4.124663(6)	8.4	5.344030(10)	9.8	−1.219366(12)	−1.41

[a] Calculated in Ref. [11] from the fitted harmonic force field.
[b] Inertial defect, $\Delta_i = I_c – I_a – I_b$.
[c] Vibrational energy difference between the two states, $\Delta E = E(v_5 = 1) - E(v_6 = 1, v_9 = 1)$.

tional spectrum of the v_5/v_6v_9 interacting dyad in $ClONO_2$. The analysis is based on a new near 'complete' spectrum in the 78–378 GHz region. It is our goal to be able to synthesize on a line-by-line basis (including hot bands and isotopologues) the rotational structure of as many infrared bands as possible. Even with the small effective integration times ($\sim 10^{-3}$ s) used to date for most of this work, the sensitivity of the system is such that we expect to reach a clutter limit. Accordingly, we have assigned the lowest energy vibrational states first so that lines associated with them can be removed from the assignment pool as we extend our work to higher states. Based on the states for which we have at least preliminary analyses [32], we expect that these simulations will be possible through at least $v_4 = 1$ at ~ 780 cm^{-1} without the use of deconvolution techniques. Preliminary work on intensity calibrations that would significantly aid such deconvolution is encouraging. However, the growing density of states that takes place with increasing vibrational energy is expected to increase the impact of perturbations and to make assignment and analysis more challenging at the level of the measurement accuracy of the microwave techniques.

Acknowledgments

We thank Manfred Winnewisser for assistance in the preparation of the chlorine nitrate and NASA for its support of this work.

Appendix A. Supplementary data

Supplementary data associated with this article are available on ScienceDirect (www.sciencedirect.com) and as part of the Ohio State University Molecular Spectroscopy Archives (http://msa.lib.ohio-state.edu/jmsa_hp.htm).

References

[1] R.D. Suenram, D.R. Johnson, J. Mol. Spectrsoc. 65 (1977) 239–248.
[2] A. Goldman, C.P. Rinsland, J.-M. Flaud, J. Orphal, J. Quant. Spectrosc. Radiat. Transfer 60 (1998) 875–882.
[3] C.P. Rinsland, M.R. Gunson, M.C. Abrams, R. Zander, E. Mahieu, A. Goldman, et al., J. Geophys. Res. 99 (1994) 18895–18900.
[4] J.L. Domenech, J.-M. Flaud, G.T. Fraser, A.M. Andrews, W.J. Lafferty, P.L. Watson, J. Mol. Spectrosc. 183 (1997) 228–233.
[5] J. Orphal, M. Morillon-Chapey, A. Diallo, G. Guelachvili, J. Phys. Chem. A101 (1997) 1062–1067.
[6] D.G. Johnson, J. Orphal, G.C. Toon, K.V. Chance, W.A. Traub, K.W. Jucks, et al., Geophys. Res. Lett. 23 (1996) 1745–1748.
[7] R.H. Miller, D.L. Bernitt, I.C. Hisatsune, Spectrochim. Acta A23 (1967) 223–236.
[8] W. Bell, G. Duxbury, D.D. Stuart, J. Mol. Spectrosc. 152 (1992) 283–297.
[9] S. Xu, T.A. Blake, S.W. Sharp, J. Mol. Spectrosc. 175 (1996) 303–314.
[10] R.D. Suenram, F.J. Lovas, J. Mol. Spectrosc. 105 (1984) 351–359.
[11] H.S.P. Muller, P. Helminger, S.H. Young, J. Mol. Spectrosc. 181 (1997) 363–378.
[12] R.A.H. Butler, S. Albert, D.T. Petkie, P. Helminger, F.C. De Lucia, J. Mol. Spectrosc. 213 (2002) 8–14.

[13] R.A.H. Butler, D.T. Petkie, P. Helminger, F.C. De Lucia, J. Mol. Spectrosc. 220 (2003) 150–152.
[14] D.T. Petkie, R.A.H. Butler, P. Helminger, F.C. De Lucia, J. Mol. Struct. 695–696 (2004) 287–293.
[15] A. Goldman, C.P. Rinsland, A. Perrin, J.-M. Flaud, J. Quant. Spectrosc. Radiat. Transfer 60 (1998) 851–861.
[16] J. Ballard, W.B. Johnston, M.R. Gunson, P.T. Wassell, J. Geophys. Res. 93 (1988) 1659–1665.
[17] J.M. Flaud, J. Orphal, W.J. Lafferty, M. Birk, G. Wagner, J. Geophys. Res. Atmos. 107 (2002) 4782.
[18] D.T. Petkie, T.M. Goyette, P. Helminger, H.M. Pickett, F.C. De Lucia, J. Molec. Spectrosc. 208 (2001) 121–135.
[19] D.T. Petkie, P. Helminger, B.P. Winnewisser, M. Winnewisser, R.A.H. Butler, K.W. Jucks, et al., J. Quant. Spectrosc. Rad. Trans. 92 (2005) 129–141.
[20] D.T. Petkie, T.M. Goyette, R.P.A. Bettens, S.P. Belov, S. Albert, P. Helminger, et al., Rev. Sci. Instrum. 68 (1997) 1675–1683.
[21] R.A.H. Butler, S. Albert, P. Helminger, F.C. De Lucia, OSU Int. Symp. Mol. Spectrosc. 54 (1999) 161.
[22] R.A.H. Butler, M. Winnewisser, F.C. De Lucia, D. Petkie, P. Helminger, OSU Int. Symp. Mol. Spectrosc. 57 (2002) 246.
[23] G. Brauer, Handbuch der Praparativen Anorganischen Chemie, vol. 1, Enke Verlag: Stuttgart.
[24] J.A. Davidson, C.A. Cantrell, R.E. Shetter, A.H. McDaniel, J.G. Calvert, J. Geophys. Res. 92 (1987) 10921–10925.
[25] J.K.G. Watson, in: J.R. Durig (Ed.), Vibrational Spectra and Structure, vol. 6, Elsevier, New York/Amsterdam, 1977, pp. 1–89.
[26] H.M. Pickett, SPFIT/SPCAT package, http://spec.jpl.nasa.gov.
[27] H.M. Pickett, J. Mol. Spectrosc. 148 (1991) 371–377.
[28] Z. Kisiel, L. Pszczolkowski, I.R. Medvedev, M. Winnewisser, F.C. De Lucia, E. Herbst, J. Mol. Spectrosc. 233 (2005) 231–243.
[29] Z. Kisiel, PROSPE—Programs for ROtational SPEctroscopy, http://info.ifpan.edu.pl/~kisiel/prospe.htm.
[30] Z. Kisiel, L. Pszczolkowski, G. Cazzoli, L. Cotti, J. Mol. Spectrosc. 173 (1995) 477–487.
[31] C.D. Esposti, A. Fuganti, Z. Kisiel, F. Tamassia, J. Mol. Spectrosc. 191 (1998) 316–325.
[32] R.A.H. Butler, Millimeter and Submillimeter Spectra of Glycolaldehyde and Chlorine Nitrate. Ph.D. Thesis, The Ohio State University, Columbus, 2002.